Accepted Manuscript

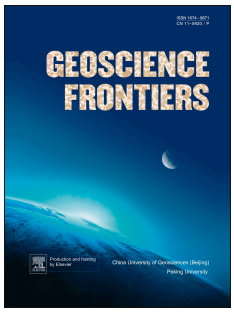

Formation of transgressive anorthosite seams in the Bushveld Complex via tectonically induced mobilisation of plagioclase-rich crystal mushes

Wolfgang D. Maier, B.T. Karykowski, Shanghong Yang

PII: S1674-9871(16)30061-5

DOI: 10.1016/j.gsf.2016.06.005

Reference: GSF 466

To appear in: *Geoscience Frontiers*

Received Date: 28 March 2016

Revised Date: 14 June 2016

Accepted Date: 17 June 2016

Please cite this article as: Maier, W.D., Karykowski, B.T., Yang, S., Formation of transgressive anorthosite seams in the Bushveld Complex via tectonically induced mobilisation of plagioclase-rich crystal mushes, *Geoscience Frontiers* (2016), doi: 10.1016/j.gsf.2016.06.005.

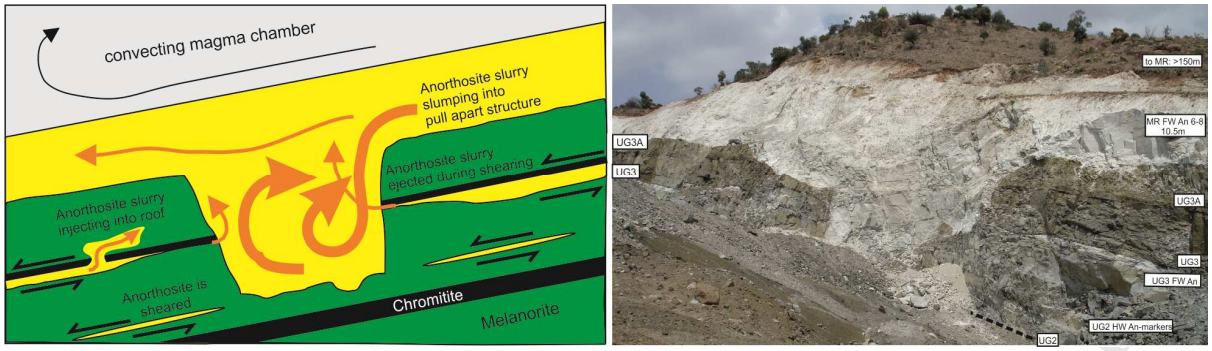

Formation of transgressive anorthosite seams in the Bushveld Complex via tectonically induced mobilisation of plagioclase-rich crystal mushes

Wolfgang D. Maier[a,*], B.T. Karykowski[a], Shanghong Yang[b]

[a] School of Earth and Ocean Sciences, Cardiff University, UK

[b] Oulu Mining School, University of Oulu, Finland

* Corresponding author e-mail address: maierw@cardiff.ac.uk

Abstract

The formation of anorthosites in layered intrusions has remained one of petrology's most enduring enigmas. We have studied a sequence of layered chromitite, pyroxenite, norite and anorthosite overlying the UG2 chromitite in the Upper Critical Zone of the eastern Bushveld Complex at the Smokey Hills platinum mine. Layers show very strong medium to large scale lateral continuity, but abundant small scale irregularities and transgressive relationships. Particularly notable are irregular masses and seams of anorthosite that have intrusive relationships to their host rocks. An anorthosite layer locally transgresses several 10 s of meters into its footwall, forming what is referred to as a "pothole" in the Bushveld Complex. It is proposed that the anorthosites formed from plagioclase-rich crystal mushes that originally accumulated at or near the top of the cumulate pile. The slurries were mobilised during tectonism induced by chamber subsidence, a model that bears some similarity to that generally proposed for oceanic mass flows. The anorthosite slurries locally collapsed into pull-apart structures and injected their hostrocks. The final step was down-dip drainage of Fe-rich intercumulus liquid, leaving behind anorthosite adcumulates.

Keywords: Anorthosite, Layered intrusion, Bushveld Complex, South Africa, Chromitite

1. Introduction

The petrogenesis of anorthosites has remained one of petrology's most controversial topics. Perhaps the key question is how to form a near-monomineralic plagioclase rock from basaltic magma that crystallises, during most stages of its fractionation, along cotectics and eutectics. Models advanced in the past include flotation of relatively light plagioclase (Kushiro, 1980), expulsion of buoyant or dense residual liquid during crystallisation (Morse, 1986; Scoates et

al., 2010), oscillating supersaturation of pyroxene and plagioclase (Maaløe, 1978; Morse, 1979a,b), shifting of phase boundaries due to pressure changes in the magma (Naslund and McBirney, 1996), volatile flux through semi-consolidated cumulates (Nicholson and Mathez, 1992), crystallisation from plagioclase saturated melt generated via resorption of suspended plagioclase (Hess, 1960) and intrusion of plagioclase mushes derived from staging chambers (Czamanske and Bohlen, 1990). The model of plagioclase flotation, in combination with subsequent diapiric ascent of plagioclase crystal mushes, has been widely accepted for massif-type anorthosites (Ashwal, 1990 and references therein), but none of the above models can readily explain the enormous lateral extent (up to several 10 s of kilometers) and knife sharp lower and upper contacts of many anorthosite seams in layered intrusions. This has led some authors to suggest that anorthosite layers formed through sorting of crystal slurries moving along the side walls and bottom of magma chambers. Irvine et al. (1998) drew analogies to turbulent density currents, whereas Maier et al. (2013) preferred a less dynamic model whereby noritic slurries were sorted and unmixed during their sliding and slumping along the top of the cumulate pile towards the centre of intrusions, triggered by crustal subsidence and accompanying seismicity. For the formation of anorthosite adcumulates which constitute a significant proportion of layered anorthosites both models additionally require drainage of residual liquid (Scoates et al., 2010).

In the present paper, we report further on our initial description (Maier et al., 2013) of a large anorthosite pothole as well as adjacent intrusive anorthosite at Smokey Hills platinum mine on the farm Maandagshoek in the eastern Bushveld Complex (Fig. 1A). The evidence presented suggests that these structures formed in response to a combination of crystal sorting during slumping of noritic slurries, downward transgression of these slurries across largely consolidated cumulate layers, and intrusion into a partially solidified crystal pile.

2. Regional geology and stratigraphy

The farm Maandagshoek is the discovery site of platinum in the Bushveld Complex (Merensky, 1926). Platinum nuggets were found in a stream running through the centre of the farm in June 1924, by farm owner AF Lombaard and Hans Merensky, leading shortly thereafter to the discovery of the Mooihoek pipe to the SE of the farm (Fig. 1B) and, in September 1924, the Merensky Reef, close to the discovery site of the nuggets (Fig. 1B). These discoveries ultimately led to the establishment of the multi-billion dollar South African platinum industry. Smokey Hills mine was initially opened in January 2008 to exploit the

UG2 chromitite exposed on 3 hills along the eastern boundary of the farm (Fig. 1B). After a temporary halt of operations in 2012–2014, African Thunder Platinum reopened the mine in early 2015.

The stratigraphy of the sequence in this area is summarised in Fig. 1C. The UG2 chromitite is, on average, 80 cm thick and contains around 8 ppm PGE (Gain, 1985; African Thunder Platinum internal report). It forms the largest PGE resource on Earth and is mined along >200 km of strike in the Bushveld Complex. It is underlain by ~1 m of pegmatoidal pyroxenite and harzburgite and overlain by several metres of melanorite containing disseminations and several thin stringers of chromite, the latter termed "leader seams". Several meters above the UG2 chromitite (between 1 and 4 m; Gain, 1985; African Thunder Platinum internal report) occur the so-called UG2 Hanging Wall Marker Layers, consisting of 2 thin seams of anorthosite. The seams may locally have thin chromitite stringers at their upper contact (Gain, 1985) and are located in a ~1 m layered noritic interval. Both Marker Layers are also developed at Atok mine, some 50 km to the NW of Smokey Hills mine and thus appear to be regionally broadly continuous. Another relatively feldspathic interval, consisting of a ~2 m norite and melanorite that is banded on a cm scale occurs approximately 5 m above the UG2 chromitite. This interval is overlain by a magmatic breccia, comprising numerous autoliths of melanorite, pyroxenite and anorthosite in a noritic matrix. Next is a ~60 cm anorthosite layer that forms the footwall to the UG3 chromitite throughout much of the northeastern Bushveld, i.e., from Atok to Maandagshoek (Gain, 1982; Mossom, 1986). The overlying ~25 cm thick UG3 chromitite contains approximately 3 ppm PGE (Gain, 1982), but is generally not mined in the Bushveld. Next follows approximately 5 m of melanorite that is distinctly more Ni rich than the UG3 footwall melanorite (Gain, 1985) and that contains low grade PGE mineralisation throughout (~0.5 ppm; Gain, 1985). Both the UG3 chromitite and hanging wall melanorite show a pronounced Pt enrichment relative to Pd, matched by few other layers in the Bushveld Complex.

The next prominent layers consist of the UG3a-b doublet, formed by 2 thin chromitites, each on average 12 cm wide, and located within a 1–2 m sequence of predominantly harzburgite and pyroxenite (Gain, 1985). This is overlain by a further 5 m of melanorite before the contact with a thick (up to 350 m), predominantly feldspathic, sequence is reached termed the Merensky Reef footwall sequence in the Bushveld mines. This is normally sub-divided into 8 units of which the lowermost 3 (units 8–6) are exposed at Smokey Hills mine. The base of the feldspathic sequence is knife sharp and defined by a 1–2 mm chromitite stringer that

undulates vertically on a scale of millimetres to meters, and laterally centimetres to 10 s of meters. The contact resembles that exposed at the base of the Upper Critical Zone at Cameron Section, but with mostly longer and less regular wavelengths. The chromitite is overlain by mottled anorthosite (Merensky Reef footwall 8 and 7). This interval is developed in broadly similar thickness at Atok mine, some 50 km to the NW and thus appears to be regionally largely continuous. It is overlain by so-called "spotted anorthosite" (MR footwall 6), a term used in Bushveld mines denoting a plagioclase-rich rock with up to around 10% cumulus pyroxene. This in turn grades upwards into norite (MR footwall 5).

3. New field observations

The bulk of the studied sequence is exposed on the slopes of Hills 2 and 3 at Smokey Hills Mine (Fig. 1B), notably in several opencast pits, of which the largest is shown in Fig 2. The UG2 seam is not accessible in most of the open pits due to their partial refill with waste, but it is well exposed along the access road to the mine.

3.1 UG2 Chromitite

The UG2 chromitite forms the base of the exposed sequence. The main seam has sharp bottom and top contacts (Fig. 3A). It is relatively undisturbed over approximately 200 m of exposure along the road cut; Major potholes are not apparent, which is notable in view of the abundance of potholes at, e.g., the UG2 exposure at Karee mine described by van der Merwe and Cawthorn (2005). However, small-scale transgressions into the footwall, somewhat analogous to those at Karee, are common, although the footwall at Maandagshoek is pyroxenite as opposed to anorthosite at Karee. Characteristic for UG2 exposures throughout the eastern Bushveld are numerous autoliths of pyroxenite and, locally, anorthosite and pegmatoid (Fig. 3). The autoliths are mostly highly elongated, with lengths up to several meters and thicknesses of mostly less than a few centimeters. They tend to be oriented parallel to the contacts of the seam. Examination of similar autoliths in 3D outcrop of chromitite from elsewhere (e.g., the LG6 seam at Cameron Section) suggests that many of the autoliths are disc shaped. The UG2 seam also contains cm- to dm-sized irregular masses of anorthosite intruding the chromitite and its hangingwall (Fig. 3B). In places, the upper portion of the UG2 bifurcates, resulting in a thin chromitite stringer branching off into the roof. It is our impression that the thin leader seams, located a few centimetres to decimetres above the main seam, are the result of such bifurcations.

3.2. The UG2 hanging wall marker layers

The marker layers are well exposed in the main pit (30°7'36"E, 24°35'15"S) and a subsidiary pit approximately 50 m to the N of the main pit. They consist of two laterally relatively continuous anorthosite seams, 3–30 cm in thickness, as well as numerous highly elongated schlieren of anorthosite between and, to a lesser extent, below and above the marker layers (Fig. 4). The layers appear to be nearly pure anorthosite with just a weak concentration of pyroxene mottles. The layers are hosted within a ~1 m distinctly banded interval of relatively leucocratic and melanocratic norite. Within the lower anorthosite seam there is a banded noritic-anorthositic horizon whose upper contact is itself transgressed by anorthosite (Fig. 4B). In several instances, the marker layers form cusps or flames injecting into the hanging wall (Fig. 4C, D). The cusps are pointing in a broadly northerly direction. The lower contacts of the marker layers are also irregular, but they are less transgressive than the upper contacts.

3.3. The interval between the UG2 hanging wall marker layers and the UG3 chromitite

The interval is approximately 15 m thick. It consists predominantly of melanorite (Gain, 1985), but 2–3 m below the UG3 chromitite is a relatively feldspathic, strongly banded interval containing decimetre-sized blocky autoliths of anorthosite (Fig. 5A, B). It is overlain by a poorly layered magmatic breccia consisting of similar anorthosite fragments as mentioned above, but hosted in larger melanocratic fragments that are distributed within a relatively leucocratic matrix (Fig. 5A). This breccia is also exposed in a stream gulley, approximately 1 km to the S of the mine. The breccia is overlain by the UG3 footwall anorthosite (Fig. 5A). This consists of 3 distinct horizons, namely an upper mottled portion, a central banded portion, and a lower schlieren-banded portion (Fig. 5C, D). The anorthosite locally wedges out (Fig. 5A), notably near both edges of the large anorthosite pothole (Figs. 2, 5A), and towards the N of the pit. The lower and upper contacts of the anorthosite are seemingly intrusive into the footwall norite and the hanging wall UG3 chromitite (Fig. 5C).

3.4. The UG3 Chromitite

The seam can be traced around most of hills 2 and 3 (Fig. 1). The relationship between the chromitite and its footwall anorthosite is complex. The chromitite may locally contain autoliths of anorthosite, but is elsewhere injected by rounded and flame-like protrusions of anorthosite (Fig. 5C). Above this injection the chromitite and its immediate hanging wall are slightly domed up, but the rocks approximately 1 m above the injection have a horizontal configuration. In a subsidiary pit to the S of the main pit, anorthosite forms a large irregular pod-like mass, brecciating the UG3 chromitite and its pyroxenitic and melanoritic host rocks

(Fig. 6). The UG3 chromitite is additionally intruded by pyroxenite at this locality (Fig. 6C). Notably, the UG3 chromitite does not appear to form significant potholes in the open pits, but in the stream gulley to the S of the mine the footwall anorthosite has been potholed extensively by pyroxenite with only thin basal coronas of chromitite exposed, possibly suggesting that the UG3 hanging wall pyroxenite potholed both the chromitite and its anorthositic footwall. In yet another variety of potholing, at Atok mine, both the UG3 and its footwall anorthosite may together pothole the underlying noritic rocks (Mossom, 1986).

The UG3a and b could not be studied in detail due to lack of accessible exposure. The uppermost chromitite of the sequence is represented by the thin but persistent stringer at the upper contact of the UG3 hanging wall melanorite with the Merensky Reef footwall 7–8 anorthosite (Fig. 7D).

3.5 The Merensky Reef footwall units 7-8 (FW 7-8)

Footwall 8 consists of a basal mottled anorthosite interlayered with spotted anorthosite. Footwall 7 is mottled anorthosite, grading upwards into spotted anorthosite and leuconorite of Footwall 6 and then norite (FW5). The mottled anorthosite has a heterogenous texture, containing noritic bands as well as mottled portions showing highly variable density and size of mottles (Fig. 7E). Along the length of the exposure at Smokey Hills mine, the anorthosite contains numerous bodies of pyroxenite and melanorite. Some of these bodies are pipe-like and likely represent members of the IRUP family (iron-rich ultramafic pipes), but banded melanorite possibly representing autoliths of the underlying units also occur (Fig. 7A).

On Hill 3 the Merensky Reef footwall 8-6 anorthosite forms a large transgressive pothole, approximately 20 m deep (Fig. 2). The lower trough of the pothole is 10–20 m wide, but the upper portion of the pothole is up to ~40 m wide. The anorthosite in the pothole shows a faint trough banding (Fig. 7B). The sidewalls of the lower trough are sub-vertical (Fig. 2) which suggests that brittle deformation played a role in its formation. However, the sequence on both sides of the pothole is at a broadly similar stratigraphic position, ruling out significant downward faulting associated with the pothole. The wall of the upper trough has a much shallower slope than that of the lower trough (Fig. 2). Along the southern sidewall, 2 thin slivers of mafic material, possibly iron-rich ultramafic rock, extend for several m into the pothole (Figs. 2 and 7C). In places, large blocks of the sidewall, consisting of UG3 chromitite and its hanging wall pyroxenite have been partially dislodged and are engulfed in anorthosite (Fig. 8). Along the northern sidewall the transgressive anorthosite appears to inject the side

wall above and below the consolidated UG3 pyroxenite package (Fig. 8B). The bottom contact of the pothole is also highly irregular.

3.6. Iron rich ultramafic pipes (IRUP)

IRUPs are well exposed , e.g., in the southern subsidiary pit where they occur within the UG3 footwall and hanging wall sequence, and in the NE face of hill 2 where they form irregular sub-vertical bodies within the Merensky Reef FW anorthosite (Fig. 7A). They can be several meters wide and mostly have sharp basal terminations, either within or at the basal contact of the host anorthosite. In one instance, the IRUP terminates on top of a melanorite autolith (Fig. 7A).

4. Petrography and mineral compositional data

In order to gain an improved understanding of the origin of the anorthosite we have analysed four samples, one each from the large anorthosite pothole, the UG3 footwall anorthosite, the Merensky Reef FW 8 mottled anorthosite and the Merensky Reef FW7 spotted anorthosite.

Sample 1 comprises a norite band in anorthosite, located approximately 1 m above the base of the large anorthosite pothole exposed in the main pit (see Fig. 2 for sample position, GPS 30°7'36"E, 24°35'15"S). The anorthosite is an adcumulate and has a sharp and undulating contact to the norite band. Plagioclase grains in the anorthosite reach 3–4 mm in size (but are mostly < 1 mm long), showing serrated and highly irregular grain boundaries (Fig. 9A) indicative of late magmatic or post magmatic deformation. Other evidence for deformation includes abundant undulous extinction and annealing of grains to form complex larger grains. The norite is medium grained and contains approximately 60% subhedral orthopyroxene (mostly 0.5–1 mm wide) and 40% subhedral plagioclase of broadly similar grain size (Fig. 9B). Plagioclase is preferentially concentrated in mm-wide stringers oriented sub-parallel to the contact between anorthosite and norite (Fig. 10).

Sample 2 comprises a 1 cm wide band of norite in anorthosite, located ~30 cm below the UG3 chromitite. It was collected in a subsidiary pit 200 m to the S of the large pothole (GPS 30°7'40"E, 24°35'21"S). The norite band is approximately 1 cm thick and bounded in its footwall and hanging wall by a 0.5–1 cm wide anorthosite adcumulate (Electronic Appendix 1). The hanging wall anorthosite adcumulate is overlain by faintly banded anorthosite-leuconorite that may contain large (up to 1 cm) clinopyroxene oikocrysts which are slightly elongated parallel to the layering. Plagioclase in the HW anorthosite adcumulate is typically

around 2–3 mm long, strongly foliated and almost as deformed as in the anorthosite of sample 1, but it lacks composite recrystallized grains (Fig. 9C). Orthopyroxene in the anorthosite is relatively large (up to about 3 mm), anhedral, and contains numerous sub-rounded plagioclase inclusions that appear to be less deformed than the cumulus plagioclase in norite and anorthosite, as judged by their relatively straight twin lamellae. Plagioclase in the norite band is mostly < 1 mm wide and has abundant spindle-shaped twin lamellae. Orthopyroxene in the norite band is subhedral and measures around 1 mm in width and length (Fig. 9D). In both norite and anorthosite, plagioclase is distinctly reverse zoned (Electronic Appendix 2), analogous to the results of Maier and Eales (1997) from the Merensky Reef-UG2 interval in the western Bushveld Complex (Electronic Appendix 3) which revealed reverse zoning towards slightly higher An (< 3–4 % An) in 9 of 10 cumulus plagioclase grains and 16 of 20 plagioclase inclusions in orthopyroxene. In sharp contrast to these Bushveld plagioclase grains, plagioclase in noritic and anorthositic cumulates of other layered intrusions, e.g., Rum, may show pronounced normal zoning with variations commonly around 20% An content (O'Driscoll et al., 2009).

Sample 3 is a mottled anorthosite collected approximately 2 m above the base of the Merensky Reef FW 8 anorthosite, in the same pit as sample 2. It is strongly foliated and most plagioclase grains are relatively large, typically up to around 3 mm (locally up to 5 mm) (Fig. 9E). However, plagioclase grain size is much reduced in certain 1–2 mm wide patches characterised by the presence of intercumulus pyroxene and enhanced alteration. Optical microscopy indicates a broadly similar degree of zoning as in samples 1 and 2. Although there are some spindle shaped twin lamellae and indented grain boundaries, the degree of deformation is much less than in samples 1 and 2. Many grain boundaries are approaching 120°. As in sample 2, plagioclase inclusions in orthopyroxene oikocrysts are notably less deformed than those outside the oikocrysts.

Sample 4 is a spotted anorthosite from the Merensky Reef FW 7, collected approximately 3 m above the base of the MR FW 8, in a further subsidiary pit located between sample locality 1 and 2–3. Plagioclase grains are mostly between 1 and 2 mm long (locally up to 5 mm). Foliation and deformation are moderate, i.e., few of the twin lamellae are bent, and the grains show relatively little undulous extinction. The rock contains small (<1 mm) anhedral and subhedral orthopyroxenes (Fig. 9F) and large oikocrysts of clinopyroxene.

Mineral compositions have been determined for samples 1 and 2 (Electronic Appendix 4). Anorthosite in sample 1 has slightly lower An contents than norite (73.4 vs 74.5) and Mg# of orthopyroxene is also slightly lower (78.9 vs 80.2). No zonation is apparent using optical microscopy or SEM. In sample 2, mean anorthite content of plagioclase in norite is 76.8, slightly higher than in sample 1, whereas $Mg^{\#}$ of orthopyroxene is 79.9, similar to sample 1. In general, plagioclase has very similar compositions as in norite and anorthosite of the UG2-Merensky Reef interval in the western Bushveld Complex (Maier and Eales, 1997). We cannot confirm the findings of Gain (1985) who reported strongly elevated anorthosite content (>83%) in plagioclase within the UG3 footwall anorthosite. Our anorthosite contents (and $Mg^{\#}$ of opx) are, however, broadly similar to those of Mondal and Mathez (2007) who found An values between 70 and 75% and $Mg^{\#}$ of orthopyroxene around 80 in the interval between the UG2 and UG3 chromitites. A further notable result of the element mapping of samples 1 and 2 is the lack of An contents below 60 and $Mg^{\#}$ below 75, suggesting very effective draining of the most differentiated residual liquids. It is presently not known to what degree this feature is unique to the Upper Critical Zone, or the Bushveld Complex as a whole.

In the present study, we did not determine whole rock compositions of our samples. The data of Maier and Eales (1997) indicate that UCZ anorthosite and norite has very low incompatible trace element contents, e.g., an average of 3.9 ppm Zr in 25 samples, suggesting <5% trapped liquid component. This is consistent with very effective removal of intercumulus liquid, or adcumulus growth at the top of the crystal pile.

5. Summary and interpretation of key observations

(1) The ~20 m interval between the UG2 chromitite and the Merensky Reef footwall 7-8 anorthosite in the eastern Bushveld Complex is prominently layered, with individual units displaying well developed lateral continuity on a scale of kilometers to 10s of km. However, exposure of the sequence at Smokey Hills mine on the farm Maandagshoek indicates that on a scale of centimetres to meters lateral continuity is poor, showing strong thickness variation, abundant transgressive relationships between layers, and numerous intrusive bodies of anorthosite and ultramafic rock (Figs. 3–8). Following Maier et al. (2013) and Forien et al. (2016) we interpret the broader scale layering to have formed through hydrodynamic sorting and kinetic sieving of crystal slurries. The main arguments are of structural and compositional nature; First, the abundant slumping- and syn-magmatic deformation structures in the Upper Critical Zone show strong similarities to those in oceanic mass flows interpreted

to have been deposited from liquefied sediments surging down sloped continental shelves. Second, the enrichment of PGE and sulphides at the ultramafic base rather than the mafic top of cyclic units is inconsistent with the strongly S undersaturated nature of Bushveld parent magmas (c.f., Barnes et al., 2010) and is more readily explained by efficient redistribution of sulphides that originally accumulated in the more fractionated portions of units. Based on intrusive relationships of certain ultramafic layers with regard to their hanging wall, Maier and Barnes (2008) and Maier et al. (2013) further argued that ultramafic and anorthositic crystal slurries may locally inject in a sill-like manner into the semi-consolidated cumulate package while they slide down along the top of the crystal pile.

(2) The stratigraphy of the UG2 hanging wall sequence at Smokey Hills mine shows some important differences to that in the western Bushveld Complex (Maier and Eales 1997); The ultramafic sequence above the UG2 chromitite is mostly around 10 m thick in the western Bushveld, whereas it measures around 20 m in the eastern Bushveld. Also, the UG3 chromitite seams are not developed in the west and the UG2 main seam is instead overlain by several so-called "leader seams" that may have thicknesses of centimeters to decimetres, show local bifurcation, and may be located up to several meters above the main seam (Leeb-du Toit, 1986). It is suggested that the UG3 seams at Smokey Hills mine are the stratigraphic equivalents of the UG2 leader seams in the western Bushveld.

(3) In common with many of the most strongly layered intervals of the Bushveld Complex, the Smokey Hills sequence contains abundant autoliths, notably within the UG2 chromitite and a noritic interval below the UG3 chromitite that resembles a magmatic breccia (Fig. 5A,B). These observations are consistent with previous studies which proposed that the UG2 unit represents an interval of particularly vigorous magma replenishment (Eales et al., 1986, 1988; Naldrett et al., 1986, 2012; Maier et al., 1994; Maier and Eales, 1997), partially eroding the top of the cumulate pile. Replenishment of the chamber with fertile magma is also consistent with the high PGE content of the UG2 unit relative to the underlying units (Gain, 1985).

(4) Anorthosite layers at Smokey Hills mine show transgressive and irregular contacts with both their hanging wall and footwall rocks (Figs. 4–8). We argue that this reflects sill-like injection of anorthositic magmas into a largely consolidated cumulate package. Unambiguous anorthosite injection, as well as potholing of pyroxenite and chromitite by anorthosite, is particularly prominent where the sequence is locally thinned, the latter interpreted to result

from down-dip syn-magmatic stretching of the cumulates. In some cases, field observations such as the flame-like anorthosite tongues in chromitite (Fig. 5C) suggest that both the anorthosite and its chromitite hanging wall were crystal mushes during injection, but adjacent to the large pothole seemingly consolidated UG3 chromitite is brecciated by intrusive anorthosite (Fig. 8). Thus the combined field data suggest that anorthosite and chromitite layers formed broadly simultaneously.

(5) Highly elongated schlieren of anorthosite within the UG2 hanging wall marker horizon (Fig. 4), noritic schlieren within the UG3 footwall anorthosite (Fig. 5D) and elongated autoliths of pyroxenite within the UG2 chromitite (Fig. 3) all imply layer-parallel ductile deformation. Micro textural observations also reveal widespread deformation features including stringers of plagioclase within norite lenses in pothole anorthosite (Fig. 10), undulous extinction, sub-grain formation and spindle twins in plagioclase (Fig. 9). The absence of significant fracturing and hydrothermal alteration suggest that deformation occurred syn-magmatically, at a relatively high temperature.

(6) The present study provides new insight into the origin of potholes. Of particular interest is the large anorthosite pothole (Fig. 2), considering that anorthosite potholes are relatively rare in layered intrusions. Eales et al. (1988) have proposed that potholes form through thermo-chemical-mechanical erosion of footwall cumulates by relatively primitive replenishing magma. However, formation of the present anorthosite pothole via thermo-chemical erosion of ultramafic cumulates would require the existence of superheated anorthositic magma, perhaps formed during depressurisation of ascending feldspathic slurries (Naslund and McBirney, 1996). We consider this model to be improbable as assimilation of ultramafic floor cumulates would drive the composition of the magma towards the cotectic with pyroxene, inconsistent with the development of thin intrusive seams and transgressive cusps of anorthosite within norite, pyroxenite and chromitite.

The anorthosite pothole has sub-vertical sidewalls suggesting that its formation was structurally controlled. The location of the pothole above a thinned cumulate succession could suggest that the formation of the pothole is related to stretching of the footwall rocks, possibly triggered by subsidence of the centre of the intrusion in response to crustal loading (Maier et al., 2013) locally leading to failure and pull-apart structures into which anorthositic crystal mushes slumped. The vortex of the slumping magma potentially widened the pothole and caused undercuts and dismemberment of the sidewalls, particularly at layer contacts. A

model of within-layer penetrative strain is consistent with the observed thinning of the sequence towards the pinch of a pinch and swell structure. In broad terms, the pothole resembles a boudin gap or pull apart extension progressively filled by relatively less viscous matrix material. Pull apart structures typically have regular sub-vertical walls, but they may locally show irregular boudin ends informally called fish mouths, resembling the sidewalls of the pothole (Fig. 8C). The anorthosite pothole thus presents a rare and unique snapshot of the early stages of formation of large potholes. Intriguingly, the UG3 footwall anorthosite pinches out on both sides of the pothole (Fig. 2). Anorthosite tends to be more competent than mafic rocks (Svahnberg, 2010) and thus the pinching out suggests that the anorthosite in the seam was incompletely solidified at the time of stretching and pothole formation. This may have allowed tectonic expulsion of the anorthosite magma. In contrast, the bulk of the remainder of the sequence was apparently largely solidified, as indicated by the angular chromitite-pyroxenite autoliths in the pothole.

(7) The formation of anorthosite adcumulates, at Smokey Hills mine (Fig. 9A,C,E; Electronic Appendix 1) and elsewhere, remains enigmatic. Based in part on the trough-like layering in the pothole anorthosite (Fig. 7B) we argue that the intruding magma was a slurry containing abundant plagioclase crystals. This model is consistent with many of the macroscopic and microscopic textures observed (Fig. 9A). Assuming that the cotectic ratio between plagioclase and pyroxene is approximately 60:40, it can be estimated that a basalt with ~50 % suspended plagioclase crystals (the maximum crystal content permissive in a flowing mush; Paterson, 2009) would solidify to have approximately 20% pyroxene. This is clearly in excess of the pyroxene content of the studied anorthosites which contain mostly < 5% pyroxene. Thus, either the anorthosites crystallised from a magma containing both a high crystal load of plagioclase and a liquid component supersaturated in plagioclase, or a large amount of residual liquid was drained from the plagioclase-rich mush prior to solidification, possibly in a down-dip direction (Scoates et al., 2010). In the absence of clear evidence for the presence of plagioclase supersaturated magma, in the Bushveld Complex and elsewhere, we favour the model of rapid and efficient draining of residual liquid. This model is consistent with the general paucity in incompatible trace elements in Bushveld anorthosite (Maier and Eales, 1997) and it shares certain features with that generally favoured for the formation of anorthosite massifs, namely initial emplacement of crystal slurries, followed by downward draining of residual liquid (Scoates et al., 2010; Arndt, 2013; Maier et al., 2013).

(8) The ubiquitous reverse zonation of plagioclase is perplexing and has been explained by equilibration of the grains with a late percolating hydrous melt that led to preferential resorption of albite component (Boudreau, 1988; Maier, 1995). Maier (1995) has shown that the fluids may be locally concentrated to form phlogopite-rich oikocrysts of olivine and pyroxene. Whether reversed zonation of plagioclase is unique to the Bushveld Complex, or to the UG2-Merensky Reef interval, remains presently unclear. In their study of 11 Upper Zone and Main Zone plagioclase grains, Tanner et al. (2014) found subdued zonation (mostly <4% An variation across grains), with just 4 of the grains being reversed zoned. The Bushveld Complex is an order of magnitude larger than other layered intrusions, and thus likely cooled slower. This could have led to relatively prolonged mobility of late magmatic hydrous fluid, followed by effective melt drainage in response to chamber subsidence. The effects of potentially elevated CO_2 in the magma, derived from devolatisation of the Transvaal dolomites in the floor of the intrusion also remain poorly studied. The solubility of CO_2 in basalt is relatively low (up to ~0.2 wt.%; Wallace et al., 2015), so the effect on the T of the plagioclase solidus would possibly be minor, but the presence of CO_2 bubbles in the flowing crystal mush could dramatically lower melt viscosity (Lesher and Spera, 2015) thereby facilitating sorting and compaction of the crystal mush, and residual melt expulsion.

(9) Transgressive ultramafic bodies, likely belonging to the ITUP family, are abundant at Smokey Hills mine and in its vicinity, e.g., at the nearby Mooihoek and Driekop pipes (Scoon and Mitchell, 2011). The field data suggest an important component of horizontal or downward movement of the IRUP magma (e.g., Fig. 12 in Maier et al., 2013). It is presently unclear whether IRUPs are relatively more abundant at Smokey Hills mine and surroundings than elsewhere in the Bushveld Complex, whether this might reflect the exceptionally good outcrop conditions in the mine, or whether IRUPs are genetically related to the large anorthosite pothole. Following Scoon and Mitchell (1994) we propose that the IRUPs represent the immiscible Fe rich end-member of residual liquids drained from anorthosites, with the relatively buoyant silica and alkali rich end-member liquid having escaped into the supernatant magma column. This model is consistent with the close spatial association of IRUPs and anorthosites on Mandagshoek and elsewhere, namely on the farm Tweefontein, eastern Bushveld Complex where anorthosite and norite fragments occur within an IRUP pipe (**Electronic Appendix 5**; Boorman et al., 2003). The latter authors interpreted the pipe to have formed from upward migrating fluid, but an alternative interpretation is that it

represents collapse of an incompletely consolidated norite-anorthosite mush into a pull apart structure, followed by downward draining of Fe-rich residual liquid.

6. Sequence of deformational and intrusive events

Our observations allow us to place some constraints on the sequence of magmatic and structural events, summarised in Fig. 11. (1) Amongst the earliest events was the hot shearing leading to the formation of anorthosite schlieren in, e.g., the UG2 hanging wall marker layers, the noritic schlieren in the UG3 footwall anorthosite and the elongated pyroxenite autoliths in the UG2 chromitite, which all indicate significant layer-parallel deformation. Whether this deformation was coeval with, or postdated the formation of the macro layering of the sequence remains to be determined, e.g., by microtextural analyses using EBSD. (2) Small anorthosite potholes within norite lenses in the UG2 hanging wall marker interval are little deformed and thus likely postdated the hot shearing. The same applies to the anorthosite flames within, and the updoming of, the UG3 chromitite. This suggests that the UG3 footwall anorthosite and the UG2 hanging wall marker anorthosite layers each consist of several sub-layers that intruded at a different time. It also implies that anorthosite is one of the last rocks to solidify in the studied sequence. (3) The large anorthosite pothole formed next, following the thinning of the sequence below the pothole, related to down-dip stretching of the entire UG2 unit. (4) The pinching out of the UG3 footwall anorthosite adjacent to the pothole suggests that the former was still in a mush state when the sequence was stretched and the pothole formed. We conclude that anorthosite layers served as lubrication planes during cumulate deformation. We propose that phase sorting during the early stage of layer formation led to plagioclase rich mushes enriched in relatively light, volatile rich residual liquid. These mushes were covered by new cumulate layers. Frequent tectonism and readjustment of the chamber then led to liquefaction, mobilisation and intrusion of anorthosite mushes into zones of dilation. The paucity of incompatible trace elements in these rocks indicates very efficient draining of residual liquid prior to final solidification, forming IRUPs. The shape of the IRUPs indicates that liquid was drained parallel to the layering and downwards across the layering.

7. Analogies between continental and oceanic layered intrusions

Gabbroic intrusions at mid-ocean ridges may be layered at the cm to 10s of cm scale, often showing well developed density grading within layers but also knife-sharp boundaries between anorthosite, troctolite and ultramafic layers. Similar to the Bushveld layers, the

mineral compositions of the oceanic intrusions show little variation, inconsistent with fractionation. Instead, the formation of the layers has been interpreted through a combination of frequent magma replenishment and hot shearing of cumulates (Jousselin et al., 2012), analogous to the model proposed here for the Bushveld Complex. The main difference between the continental and oceanic intrusions is that in the latter process was driven by mantle flow rather than chamber subsidence.

8. Conclusions

Our understanding of the petrogenesis of layered intrusions, and the Bushveld Complex in particular, has made significant advances in the last decade, partly due to new exposures of the Upper Critical Zone that have become accessible in a number of open pits (e.g., van der Merwe and Cawthorn, 2005). The open pits at Smokey Hills mine are particularly revealing, being that they present up to 1 km of continuous lateral exposure of the UG2 hanging wall sequence. The characterisation and study of these rocks is still in its early stages, but initial observations allow us to propose the following preliminary petrogenetic model (Fig. 12): (1) The pronounced layering of the sequence formed largely through hydrodynamic sorting and kinetic sieving of crystal slurries at the top of the cumulate pile in response to chamber subsidence. This process resulted in distinct, sharply bound layers of chromitite, melanorite, and anorthosite and in enrichment of sulphides and PGE at the ultramafic base of units. (2) Plagioclase-rich layers contained relatively large proportions of buoyant residual liquid and thus remained incompletely solidified for a relatively long time. (3) The distinct density contrasts between layers, notably where chromitite overlaid anorthosite led to local flame-like intrusion of anorthosite mush into, and up-doming of, the hanging wall chromitite, reminiscent of load cast structures in sedimentary deposits. (4) Continued subsidence of the central portion of the intrusion in response to crustal loading caused stretching and flexing of the uppermost portion of the cumulate pile, resulting in pinch-and-swell structures. Semi-consolidated anorthosite layers located near the top of the crystal pile acted as lubrication planes facilitating structural failure and opening of pull-apart structures. (5) Hot shearing within the cumulate pile led to remobilisation of some of the buried anorthosite mushes, and injection into their footwall and hanging wall. (6) Anorthosite slurries located at the top of the cumulate pile collapsed into the pull-apart structures leading to the formation of large anorthosite potholes.

Our study concludes that layering in the Bushveld Complex and other mafic-ultramafic intrusions formed through a combination of magmatic and structural processes. Transgressive features known as potholes may be induced by extension of the subsiding cumulate pile, particularly the larger examples. Magmatic erosion of the side walls may modify the shapes of these potholes.

Many questions remain to be solved. For example, the proposed model is likely not applicable to all transgressive features, namely small sub-circular dimples described from the base of the UG2 chromitite at Karee mine (van der Merwe and Cawthorn, 2004) and elsewhere, which may have formed through thermal erosion (Campbell, 1986). Another unresolved issue is whether potholes are more common in the Bushveld Complex than in other layered intrusion, mainly because of limited exposure in the latter. The relatively larger size of the Bushveld Complex could have resulted in enhanced crustal subsidence and slower cooling, favouring mobilisation of erosive crystal slurries. A further factor could be the presence of the Transvaal dolomite platform below the Bushveld. If this released substantial CO_2 to the Bushveld magma chamber during contact metamorphism, the resulting bubbles could have resulted in significant reduction of magma viscosity (Lesher and Spera, 2012), facilitating cumulate mobilisation and footwall erosion.

9. Acknowledgements

We thank African Thunder Platinum and Smokey Hills Mine for access to their property and samples, in particular chief mine geologist Paul Herron who spent a day guiding us around the exposures. Tony Oldroyd is thanked for producing the thin sections. Constructive reviews were provided by two anonymous reviewers.

References

Arndt, N.T., 2013. The formation of massif anorthosite: Petrology in reverse, Geoscience Frontiers 4, 195–198.

Ashwal, L.D., 1990. Anorthosites, Springer Verlag, Berlin, 422pp.

Barnes, S-J, Maier, W.D., Curl, E., 2010. Composition of the marginal rocks and sills of the Rustenburg Layered Suite, Bushveld Complex, South Africa: Implications for the formation of the PGE deposits. Economic Geology 105, 1491-1511.

Boorman, S.L., McGuire, J.B., Boudreau, A.E., Kruger, F.J., 2003. Fluid overpressure in layered intrusions: formation of a breccia pipe in the eastern Bushveld Complex, Republic of South Africa. Mineralium Deposita 38, 356-369.

Boudreau, A.E., 1988. Investigations of the Stillwater Complex IV. The role of volatiles in the petrogenesis of the J-M Reef, Minneapolis adit section. Canadian Mineralogist 26, 193–208.

Campbell, I.H. , 1986. A fluid dynamic model for the potholes of the Merensky Reef. Econ Geol., 81, 1118-1125.

Czamanske, G. K., Bohlen, S. R. 1990. The Stillwater Complex and its anorthosites: an accident of magmatic underplating? American Mineralogist 75, 37-45.

Eales, H.V., Marsh, J.S., Mitchell, A.A., De Klerk, W.J., Kruger, F.J., Field, M., 1986. Some geochemical constraints upon models for the crystallization of the Upper Critical Zone-Main Zone interval, northwestern Bushveld Complex. Mineralogical Magazine 50, 567-582.

Eales, H.V., Field, M., de Klerk, W.J., Scoon, R.N., 1988. Regional trends of chemical variation and thermal erosion in the Upper Critical Zone, western Bushveld Complex. Mineralogical Magazine 52, 63-79.

Eales, H.V., De Klerk, W.J., Teigler, B., 1990. Evidence for magma mixing processes within the Critical and Lower Zones of the northwestern Bushveld Complex, South Africa., Chemical Geology 88, 261-278.

Forien, M., Tremblay, J., Barnes, S.-J., Burgisser, A., Page, P., 2016. The Role of Viscous Particle Segregation in forming Chromite Layers from Slumped Crystal Slurries: Insights from Analogue Experiments. Journal of Petrology, doi: 10.1093/petrology/egv060

Gain, S.B., 1985. The geologic setting of the platiniferous UG2 chromitite layer on Maandagshoek, eastern Bushveld Complex. Economic Geology 80, 925-943.

Hess, H.H., 1960. Stillwater igneous complex. Memoir of the Geological Society of America 80, 1-230.

Irvine, T.N., Andersen, J.C.O., Brooks, C.K., 1998. Included blocks (and blocks within blocks) in the Skaergaard Intrusion: Geological relations and the origins of rhythmic modally graded layers. Bulletin of the Geological Society of America 110, 1398-1447.

Kushiro, I., 1980. Viscosity, density, and structure of silicate melts at high pressures and their petrological applications. In: Hargraves, R.B. (Ed.), Physics of Magmatic Processes. Princeton University Press, Princeton, pp. 93–120.

Lesher, C.E., Spera, F.J., 2015. Thermodynamic and transport properties of silicate melts and magma. 113-141, In H Sigurdsson, B Houghton, S McNutt, H Rymer, J Stix (Eds), The Encyclopedia of volcanoes, Academic Press, 1422 pp.

Maaloe, S. 1978. The origin of rhythmic layering. Mineralogical Magazine 42, 337-345.

Morse, S.A., 1979a. Kiglapait geochemistry I: Systematics, sampling, and density. Journal of Petrology 20, 555-590.

Morse, S.A., 1979b. Kiglapait geochemistry II: Petrography. Journal of Petrology 20, 591-624.

Morse, S.A., 1986. Convection in aid of adcumulus growth. Journal of Petrology 27, 1183-1214.

Maier, W.D., 1995. Olivine oikocrysts in Bushveld anorthosite: some implications for cumulate formation: Canadian Mineralogist 33, 1011-1022.

Maier, W.D., Eales, H.V., 1997. Correlation within the UG2 - Merensky Reef interval of the Western Bushveld Complex, based on geochemical, mineralogical and petrological data: Geological Survey of South Africa, Bulletin 120, 56 pp.

Maier, W.D., Barnes, S-J., 2008. Platinum-group elements in the UG1 and UG2 chromitites and the Bastard reef at Impala platinum mine, western Bushveld Complex, South African Journal of Geology 111, 159-176.

Maier, W.D., Rasmussen, B., Li, C., Barnes, S-J., Huhma, H., 2013. The Kunene anorthosite complex, Namibia, and its satellite bodies: geochemistry, geochronology and economic potential. Economic Geology 108, 953–986.

Maier, W.D., Barnes, S-J, Groves, D.I., 2013. The Bushveld Complex, South Africa: Formation of platinum-palladium, chrome and vanadium- rich layers via hydrodynamic

562 sorting of a mobilized cumulate slurry in a large, relatively slowly cooling, subsiding magma
563 chamber. Mineralium Deposita 48, 1-56.

564 Merensky, H., 1926. Die neuentdeckten Platinfelder im mittleren Transvaal, und ihre
565 wissenschaftliche Bedeutung. Berliner Zeitschrift der Deutschen Geologischen Gesellschaft
566 78, 298-314.

567 Mondal, S.K., Mathez, E.A., 2007. Origin of the UG2 chromitite layer, Bushveld Complex.
568 Journal of Petrology 48, 495-510.

569 Mossom, R. J. 1986. The Atok platinum mine. In: Anhaeusser, C.R., Maske, S. (Eds.),
570 Mineral deposits of Southern Africa. Geological Society of South Africa, Johannesburg, pp
571 1143-1154.

572 Naldrett, A.J., Gasparrini, E.C., Barnes, S.J., Von Gruenewaldt, G., Sharpe, M.R., 1986. The
573 Upper Critical Zone of the Bushveld Complex and the origin of Merensky-type ores.
574 Economic Geology 81, 1105-1117.

575 Naldrett, A.J., Wilson, A., Kinnaird, J., Yudovskaya, M., Chunnett, G., 2011. The origin of
576 chromitites and related PGE mineralization in the Bushveld Complex: new mineralogical and
577 petrological constraints. Mineralium Deposita 47, 209-232.

578 Naslund, H.R., McBirney, A.R., 1996. Mechanisms of formation of igneous layering. In:
579 Cawthorn, R.G., (Ed.), Layered intrusions, Elsevier, Amsterdam, pp. 1-43.

580 Nicholson, D.M., Mathez, E.A., 1991. Petrogenesis of the Merensky Reef in the Rustenburg
581 section of the Bushveld Complex. Contributions to Mineralogy and Petrology 107, 293-309.

582 O'Driscoll, B., Donaldson, C.H., Daly, J.S., Emeleus, C.H. 2009. The roles of melt
583 infiltration and cumulate assimilation in the formation of anorthosite and a Cr-spinel seam in
584 the Rum Eastern Layered Intrusion. Lithos 111, 6–20.

585 Paterson, S.R., 2009. Magmatic tubes, pipes, troughs, diapirs, and plumes: Late-stage
586 convective instabilities resulting in compositional diversity and permeable networks in
587 crystal-rich magmas of the Tuolumne batholith, Sierra Nevada, California. Geosphere 5, 496-
588 527.

589 Scoates, J.S., Lindsley, D.H., Frost, B.R., 2010. Magmatic and structural evolution of an
590 anorthositic magma chamber: The Poe Mountain intrusion, Laramie Anorthosite Complex,
591 Wyoming. Canadian Mineralogist 48, 851-885.

592 Scoon, R.N., Mitchell, A.A., 1994. Discordant iron-rich ultramafic pegmatites in the
593 Bushveld Complex and their relationship to iron-rich intercumulus and residual liquids.
594 Journal of Petrology 35, 881-917.

595 Scoon, R.N., Mitchell, A.A., 2004. The platiniferous dunite pipes in the eastern limb of the
596 Bushveld Complex: Review and comparison with unmineralized discordant ultramafic
597 bodies. South African Journal of Geology 107, 505-520.

598 Tanner, D., Mavrogenes, J.A., Arculus, R.J., Jenner, F.E., 2014. Trace Element Stratigraphy
599 of the Bellevue Core, Northern Bushveld: Multiple Magma Injections obscured by diffusive
600 processes. Journal of Petrology 55,859-882.

601 Van der Merwe, J., Cawthorn, R.G., 2005. Structures at the base of the Upper Group 2
602 chromitite layer, Bushveld Complex, South Africa, on Karee Mine (Lonmin Platinum),
603 Lithos 83, 214-228.

604 Wallace, P.J., Plank, T., Edmonds, M., Hauri, E.H., 2015. Volatiles in magmas, 163-183. In
605 H Sigurdsson, B Houghton, S McNutt, H Rymer, J Stix (Eds), The Encyclopedia of
606 volcanoes, Academic Press, 1422 pp.

607

608 **Figure Captions**

609 Figure 1: (A) Simplified geological map of the Bushveld Complex. (B) Geological map of
610 the farm Maandagshoek, showing location of studied exposures (star symbol). (C)
611 Stratigraphic column, with average thicknesses of layers (modified from African Thunder
612 unpublished report). Peg Px = pegmatoidal pyroxenite; MN = melanorite; MGb =
613 melagabbro; An = anorthosite; No = norite; Cr = chromitite.

614 Figure 2: Large anorthosite pothole at Smokey Hills mine. View from NE, with key features
615 discussed in the text indicated.

616 Figure 3. The UG2 chromitite as exposed along the access road to Smokey Hills mine. (A)
617 Note thin elongated pyroxenite autolith in upper portion of seam, and sharp, but undulating
618 bottom contact. Inset shows lens-like pegmatoidal rock with chromitite selvage within the
619 UG2 seam, representing either an autolith or an intrusion. (B) The UG2 seam is split by a
620 large autolith of pyroxenite, locally resulting in slight updoming of the upper contact of the

seam. Also note a band of anorthosite-pyroxenite near basal contact (arrow), and pods of anorthosite associated with the leader seams (arrow at upper right).

Figure 4: The UG2 hanging wall marker layers consist of 2 anorthosite seams within a 1 m interval of banded norite. Note cusps and flames of anorthosite extending into the hanging wall norite, and several thin schlieren and lenses of anorthosite between the marker layers. (A) Overview of layered interval hosting the marker layers, (B) close-up of highlighted area from (A), with arrow pointing to small pothole of anorthosite in norite. (C+D) Further examples of anorthosite flames or cusps extending into banded hanging wall norite.

Figure 5: Rocks from the sequence between the UG2 hanging wall marker layers and the UG3 chromitite. (A) UG3 chromitite, underlain by anorthosite footwall, magmatic breccia of melanorite fragments containing anorthosite fragments within leuconoritic matrix (yellow arrow), and banded norite. (B) Banded norite containing blocky anorthosite autoliths below UG3 chromitite. (C) The UG3 footwall anorthosite seemingly injects its footwall and hanging wall. Note that anorthosite consists of upper mottled portion, central weakly banded portion, and lower schlieren-banded portion. (D) Melanorite lenses within UG3 footwall anorthosite.

Figure 6: (A) Large mass of intrusive anorthosite occurring in thinned pyroxenite-chromitite sequence of southern pit. Thinning of sequence is reflected by downwarping of UG3a+b seams. (B) Close-up of UG3 chromitite invaded by pyroxenite. (C) Fragmentation of UG3 chromitite by intruding anorthosite.

Figure 7: (A) The contact between the MR footwall 8 anorthosite and the UG3 hanging wall pyroxenite / melanorite. Note autoliths of banded melanorite on left and right (yellow arrows), and several intrusions of IRUP. (B) Trough banding (yellow stippled lines) in anorthosite within large pothole of Fig. 2. (C) Transgressive irregular contact between melanorite and anorthosite on southern sidewall of large anorthosite pothole. Note sideway extension of melanorite into the pothole (red arrow). Also note pinching out of UG3 as pothole edge is approached. (D) Contact chromitite stringer between UG3b HW pyroxenite and MR FW8 anorthosite. (E) Textural variability of MR FW8 mottled anorthosite. (f) Melanorite of UG3b hanging wall.

Figure 8: Relationships between anorthosite pothole and its sidewall. (A) Dislodgement of pyroxenite and chromitite by intruding anorthosite. (B) Intrusion of anorthosite above and below UG3 chromitite. (C) Relationships in northern portion of pothole. Note change in dip below pothole (lower yellow arrow) interpreted to result from flexure prior to pothole

formation, coincident with location of intrusive anorthosite lens (upper yellow arrow). Also note how anorthosite magma carves out the sidewall at the contact between lithologies. (D) Close-up of anorthosite lens from (C). The anorthosite forms pegmatoidal upward extensions into the norite and it contains lenses of what appears to be pegmatoidal pyroxenite, possibly IRUP.

Figure 9: Photomicrographs of analysed rocks. (A) Anorthosite, sample 1. (B) Norite, sample 1. (C) Anorthosite, sample 2. (D) Norite, sample 2. (E) Anorthosite, sample 3. (F) Anorthosite, sample 4.

Figure 10: Element map of sample 1, showing strings of plagioclase and orthopyroxene within melanorite.

Figure 11: Schematic model of formation of anorthosite pothole on Smokey Hills. See text for further explanation.

Figure 12: Sketch model of pothole formation in Bushveld Complex. In steps 1–3 layering forms due to subsidence and sorting of noritic proto cumulates. In steps 4–6, flexing of the cumulate sequence results in pull apart structures into which anorthosite slurries plunge. Also note injection of anorthosite into semi solidified cumulus sequence, notably in areas of enhanced stretching.

Electronic Appendices

ElectronicAppendix 1: Banded anorthosite-norite of sample 2. Note distinct foliation in anorthosite, expressed in the form of mm-wide bands of anorthosite and leuconorite.

Electronic Appendix 2: Element map across a norite band within anorthosite of sample 2. Note pervasive reversed zoning in plagioclase, and lack of compositional variation between anorthosite and norite.

Electronic Appendix 3: Zoning in cumulus plagioclase of the UG2-Merensky Reef interval, western Bushveld Complex

Electronic Appendix 4: Mineral compositions in samples 1 and 2 (SH1 and 2)

682 Electronic

683 Appendix 5: Breccia pipe of anorthosite-norite fragments within iron-rich ultramafic matrix
684 at Tweefontein, eastern Bushveld Complex. Contacts of pipe are delineated by persons
685 (photograph courtesy of Richard Arculus).

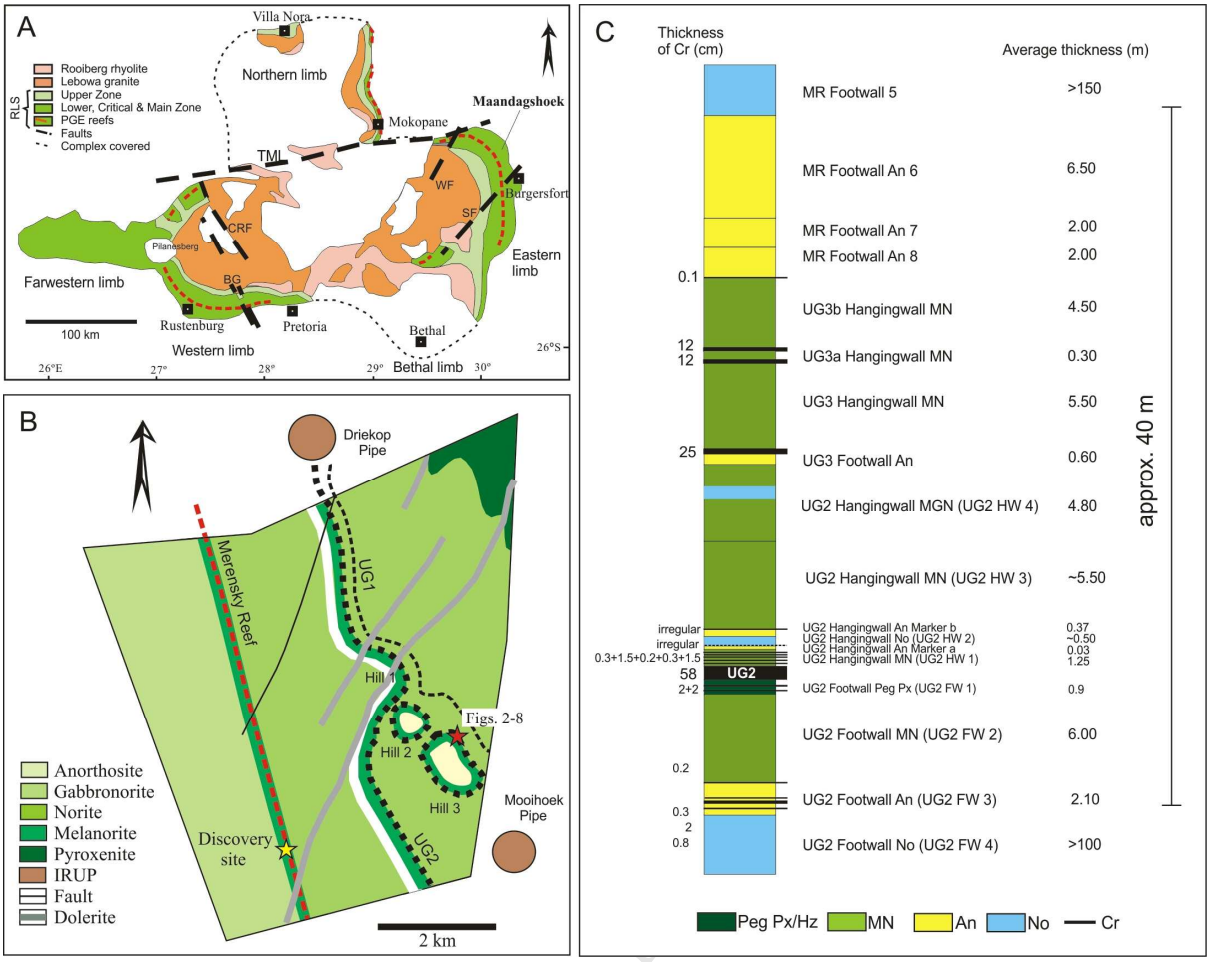

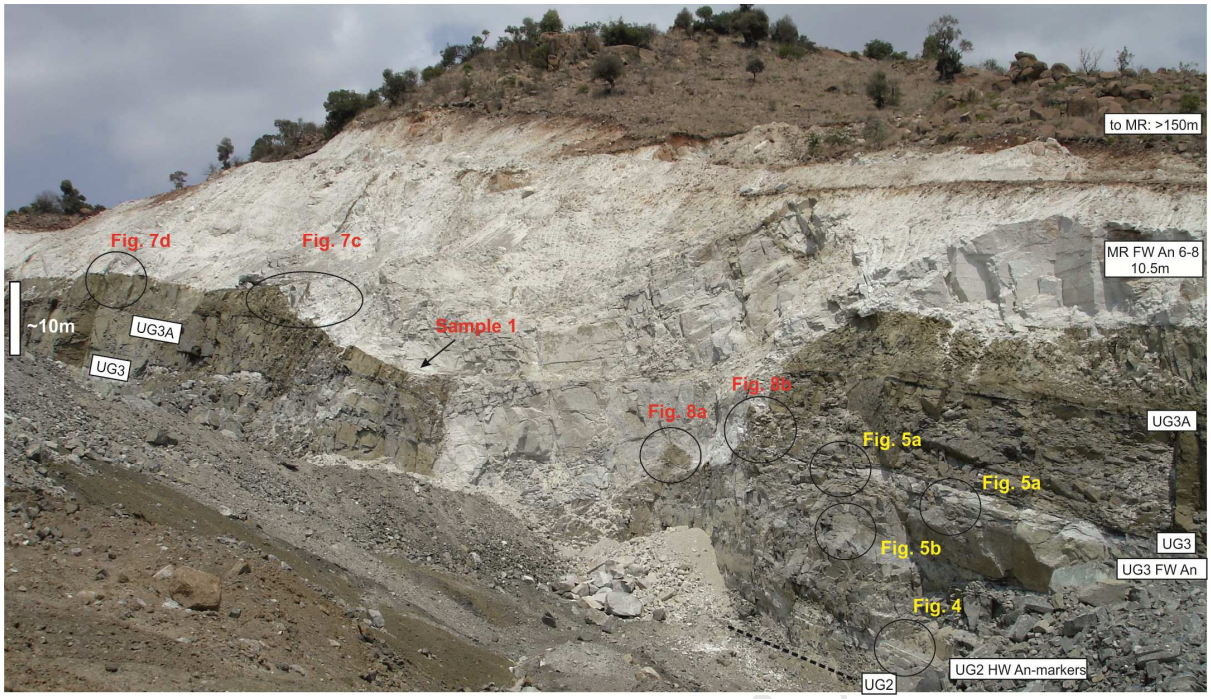

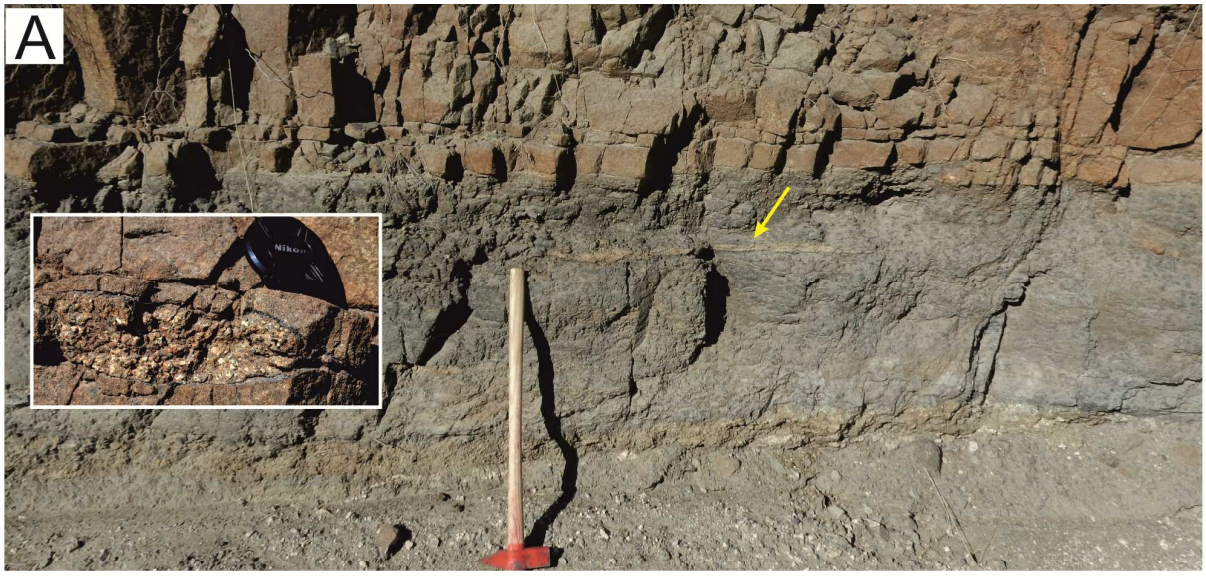

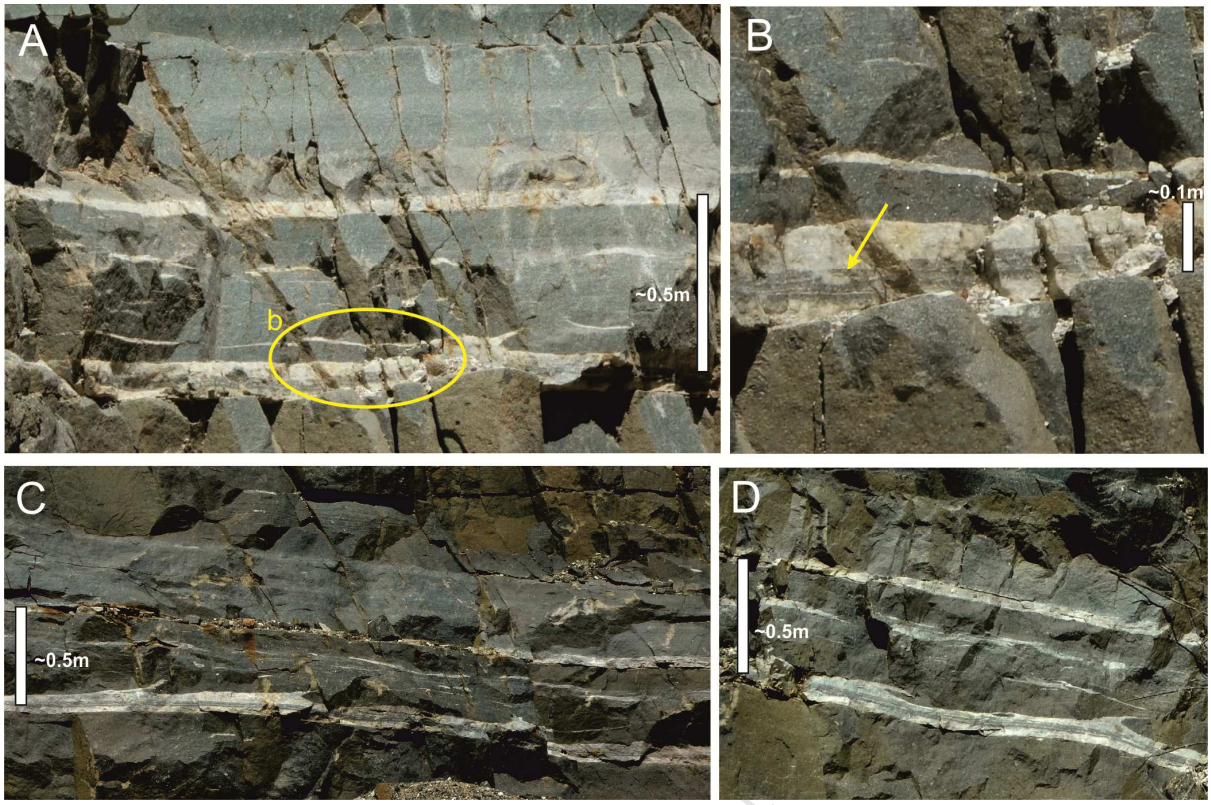

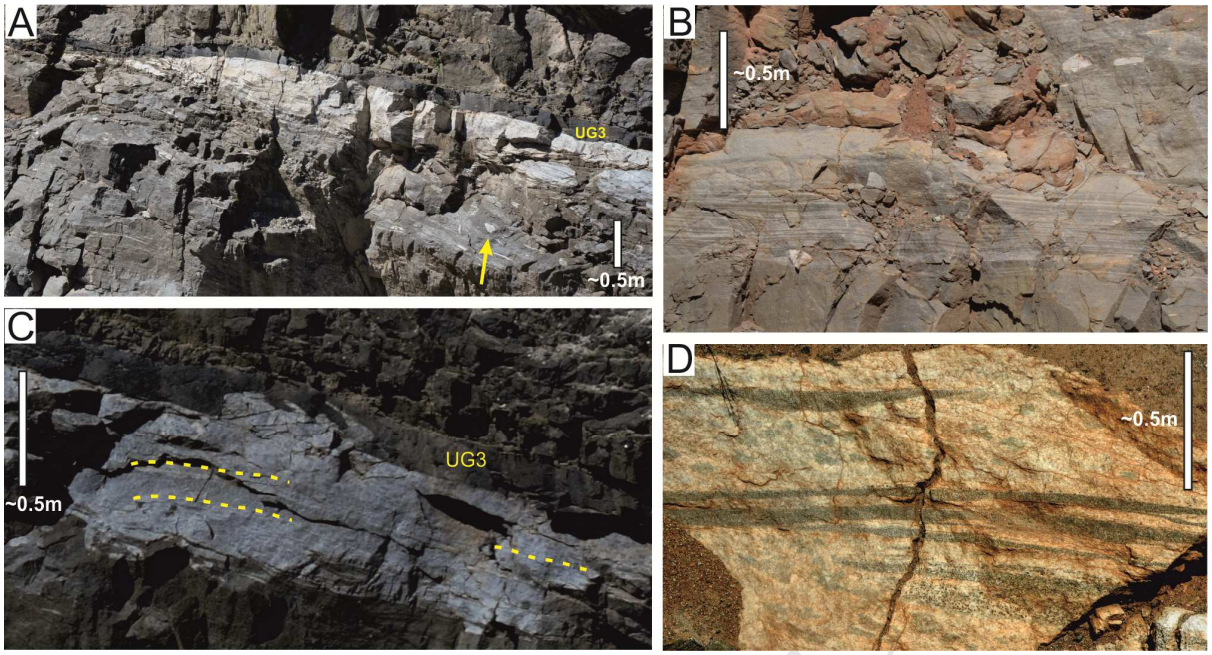

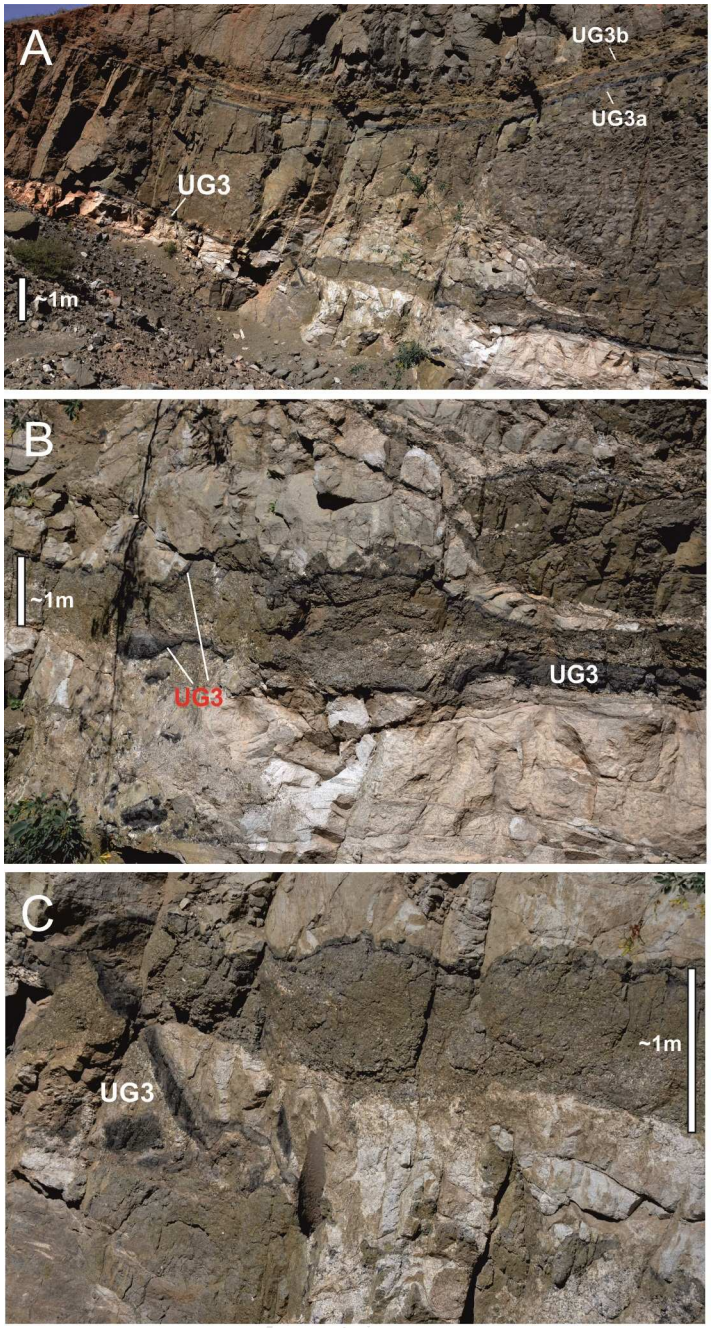

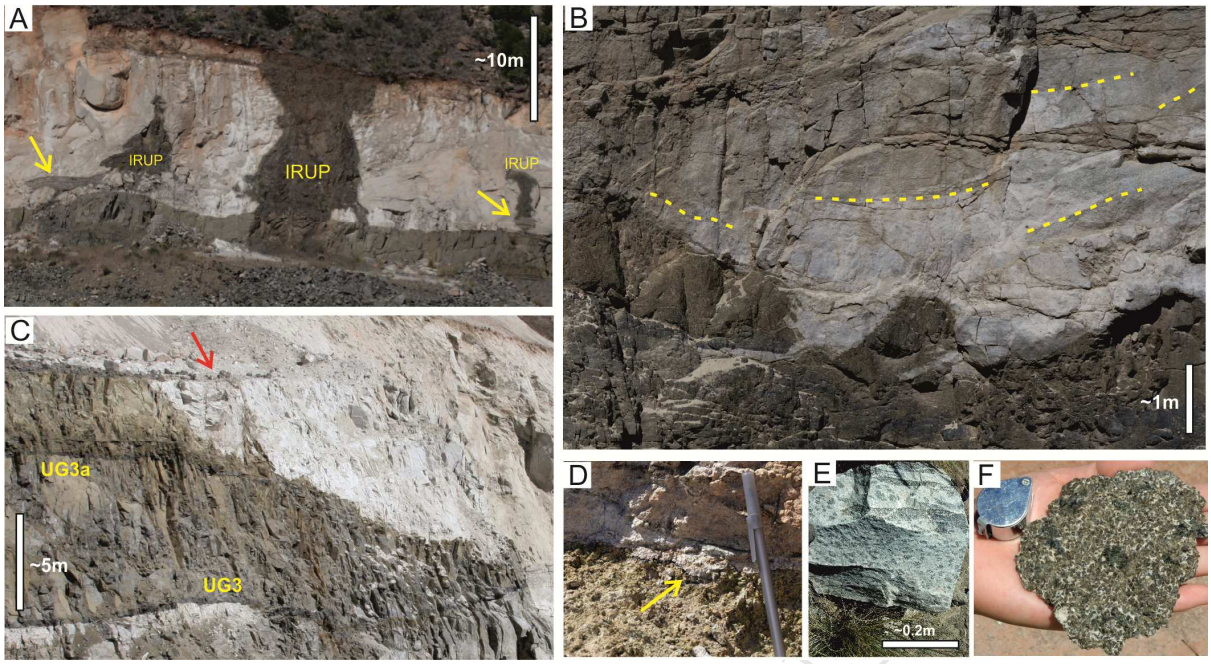

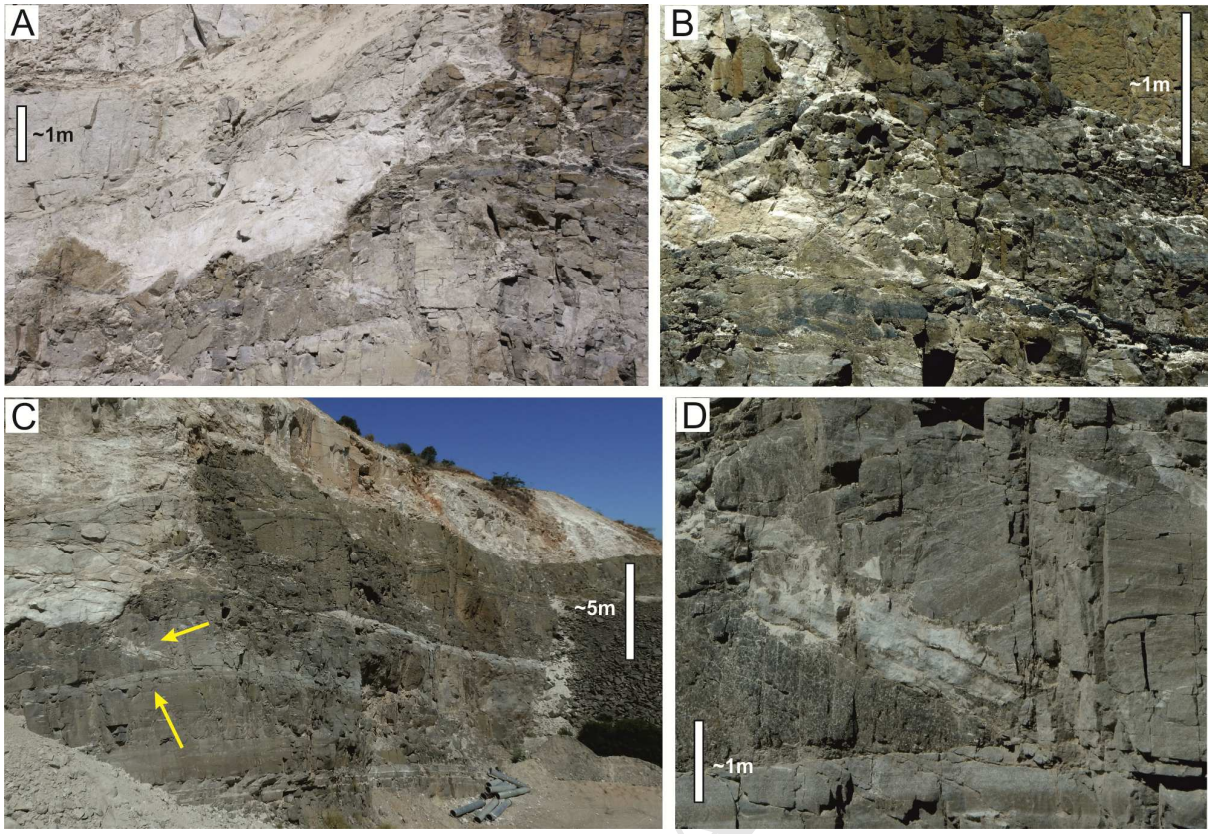

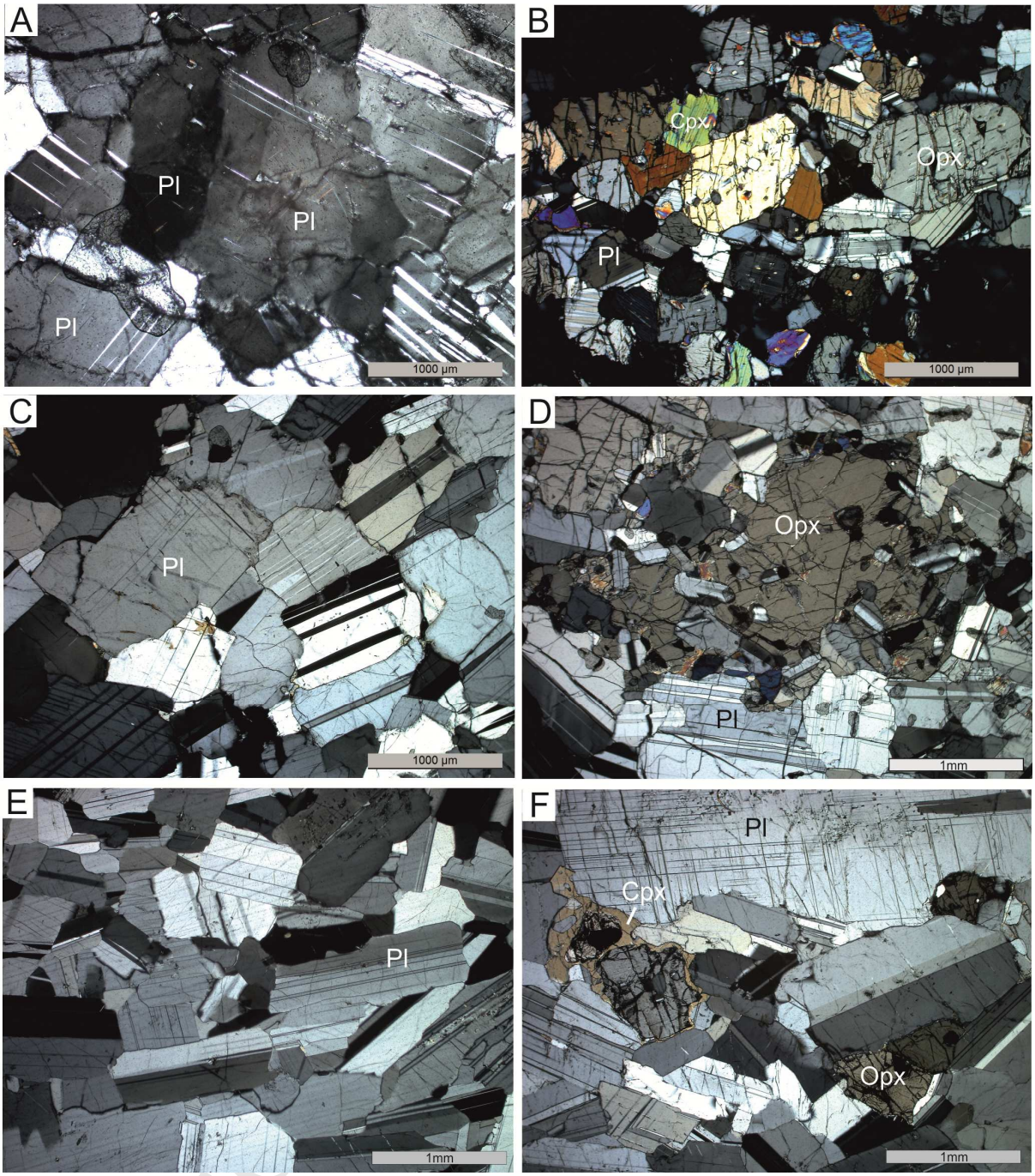
A
Pl
Pl
Pl
1000 µm
B
Cpx
Opx
Pl
1000 µm
C
Pl
1000 µm
D
Opx
Pl
1mm
E
Pl
1mm
F
Pl
Cpx
Opx
1mm

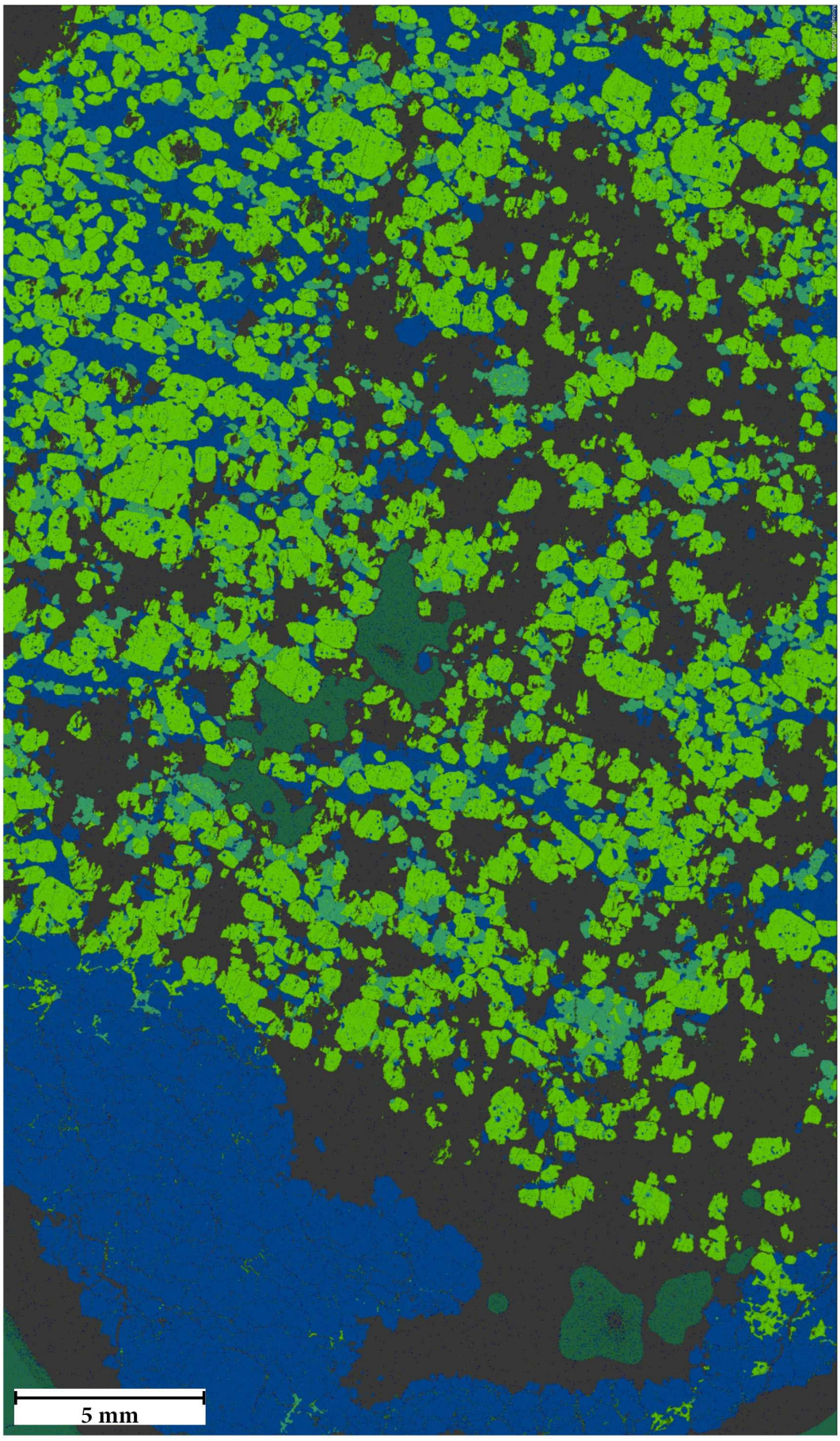
5 mm
Plagioclase
Orthopyroxene
Clinopyroxene

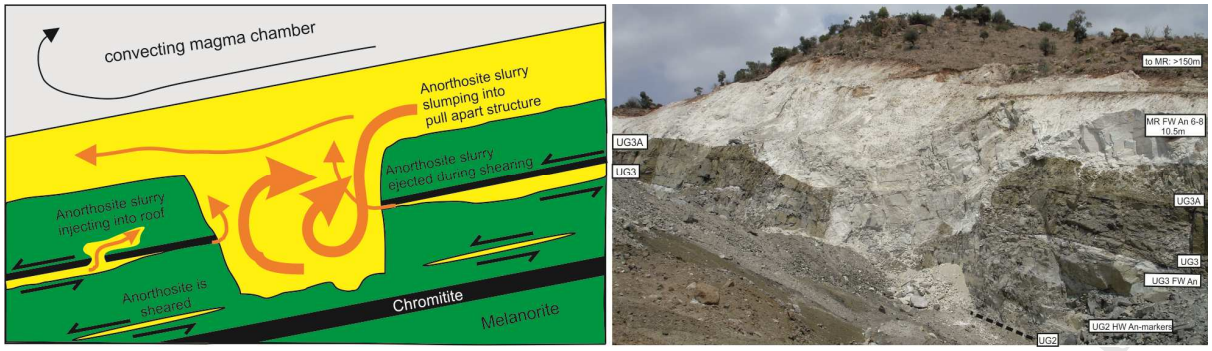

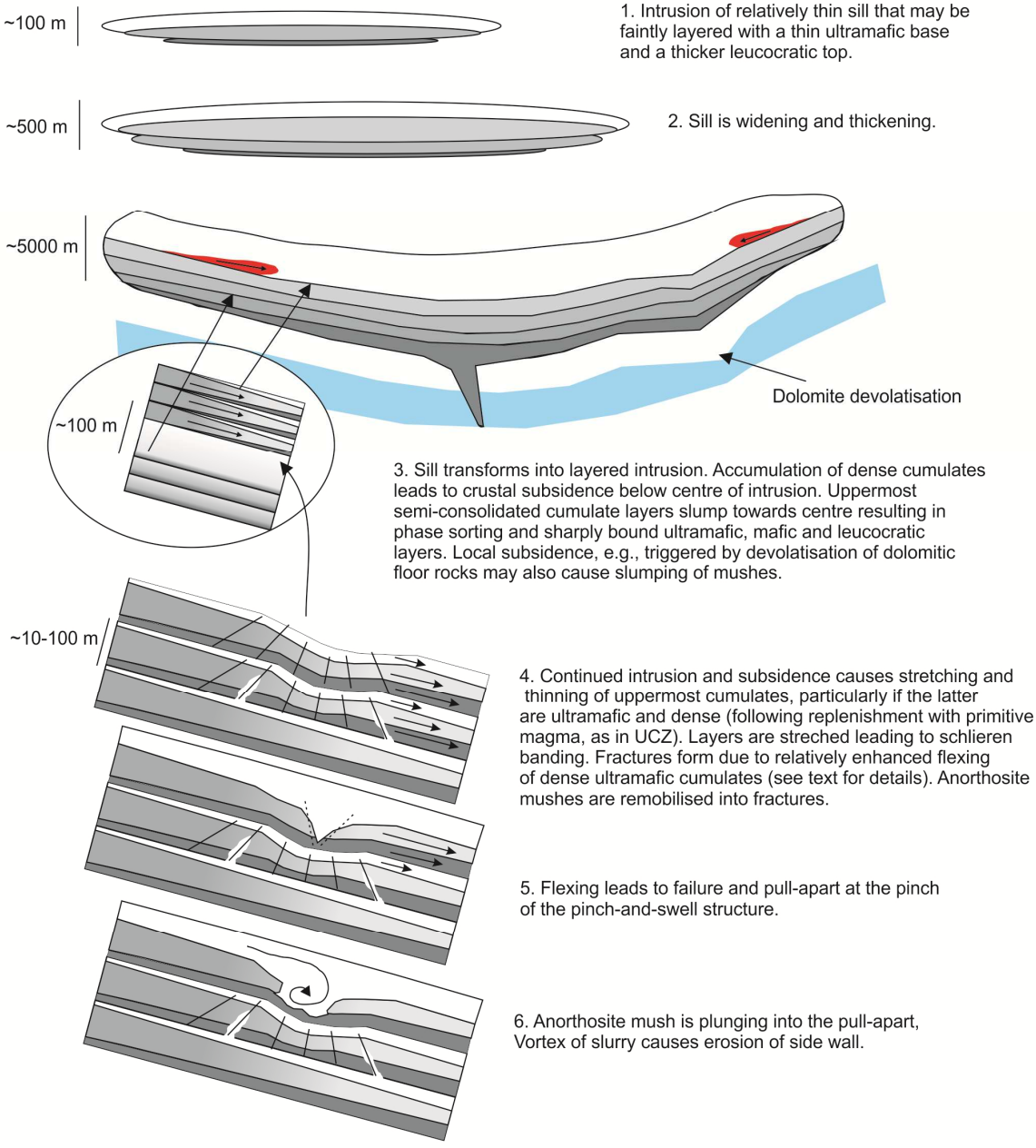
~100 m
1. Intrusion of relatively thin sill that may be faintly layered with a thin ultramafic base and a thicker leucocratic top.
~500 m
2. Sill is widening and thickening.
~5000 m
Dolomite devolatisation
~100 m
3. Sill transforms into layered intrusion. Accumulation of dense cumulates leads to crustal subsidence below centre of intrusion. Uppermost semi-consolidated cumulate layers slump towards centre resulting in phase sorting and sharply bound ultramafic, mafic and leucocratic layers. Local subsidence, e.g., triggered by devolatisation of dolomitic floor rocks may also cause slumping of mushes.
~10-100 m
4. Continued intrusion and subsidence causes stretching and thinning of uppermost cumulates, particularly if the latter are ultramafic and dense (following replenishment with primitive magma, as in UCZ). Layers are streched leading to schlieren banding. Fractures form due to relatively enhanced flexing of dense ultramafic cumulates (see text for details). Anorthosite mushes are remobilised into fractures.
5. Flexing leads to failure and pull-apart at the pinch of the pinch-and-swell structure.
6. Anorthosite mush is plunging into the pull-apart, Vortex of slurry causes erosion of side wall.

Highlights

- Anorthosites act as lubrication planes during tectonism of layered intrusions
- Mobilised plagioclase-rich slurries may form intrusive anorthosites
- Anorthositic adcumulates form through down-dip draining of Fe rich residual liquid